Transactions of the Royal Society of Edinburgh: Earth Sciences, **94**, 309–324, 2004 (for 2003)

Fluids and hydrothermal alteration assemblages in a Devonian gold-bearing hot-spring system, Rhynie, Scotland

M. Baron, S. Hillier, C. M. Rice, K. Czapnik and J. Parnell

ABSTRACT: Hydrothermal alteration at Rhynie, Aberdeenshire, Scotland, is concentrated along a fault zone, which juxtaposes surface deposits and the mineralised feeder zone to the Rhynie hot-spring system. Mineralisation consists of breccias and veins filled with quartz, chert, calcite, K-feldspar and pyrite. Associated pervasive alteration comprises a high-temperature K-feldspar-quartz-illite facies (formed at 250–350°C), a medium-temperature mixed layered illite/smectite-quartz-K-feldspar-chlorite-calcite facies (formed at 150–200°C) and a low-temperature mixed layered illite/smectite-chlorite-calcite facies (formed at 100 to +150°C). The fluids responsible for mineralisation were mainly moderate- to high-temperature (T_h=91–360°C), low-salinity (<0·2 to 2·9 wt.% NaCl eq.) H_2O-NaCl-heated meteoric fluids comparable to modern and ancient hot-spring systems. The migration of these fluids was mainly restricted to a major fault zone bounding the Devonian basin. Fluids responsible for mineralisation, alteration and cementation elsewhere in the basin were low-temperature (T_h 57 to 161°C), low- to high-salinity (<0·2 to 18 wt.% NaCl eq.) H_2O-NaCl fluids, which resemble basinal brines.

KEY WORDS: Epithermal gold mineralisation, fluid inclusions, hot springs, siliceous sinters, X-ray diffraction.

The Rhynie chert, which contains world-renowned, well-preserved remains of Early Devonian terrestrial plant and arthropod communities, has been interpreted as a hot-spring sinter (Mackie 1913; Kidston & Lang 1917). More recent geochemical work has shown that the cherts and associated hydrothermally altered rocks contain anomalous levels of elements which are known to be enriched at shallow levels in epithermal mineral deposits and some modern hot-spring systems (Rice & Trewin 1988; Rice *et al.* 1995). The most intense hydrothermal mineralisation and alteration is concentrated along the Rhynie Fault Zone (Rice & Ashcroft 2004), indicating that this structure provided the main conduit for the hydrothermal fluids which fed the hot springs.

The Rhynie basin, which is 21 km long by 3 km wide, and contains about 1 km of predominantly interbedded sandstones, shales, conglomerates, andesitic lavas and tuffs (Rice & Ashcroft 2004), is situated in Aberdeenshire, Northeast Scotland (Fig. 1). The basin is a half-graben structure bound by a faulted contact to the west and an unconformity or faulted margin to the east (BGS 1993; Gould 1997; Rice & Ashcroft 2004). Strata generally dip at shallow angles of between 15 and 30° to the northwest. The general depositional environment of the Rhynie sequence is interpreted as an alluvial plain with associated ephemeral lakes (Trewin 1994; Trewin & Wilson 2004). Over 50 beds of chert (the Rhynie Chert Unit) occur interbedded with siliceous sandstones and mudstones towards the top of succession, which represent repeated pulses of hydrothermal activity (Rice *et al.* 2002).

The Rhynie basin overlies basement rocks consisting of the Boganclough and Insch intrusions, which are comprised mainly of Ordovician quartz-biotite norites and minor serpentinites (Busrewil *et al.* 1973), emplaced in Dalradian metamorphic rocks. The Boganclough intrusion is cut by a number of basic dykes, granites and syenites of uncertain age (Rice *et al.* 1995).

In this contribution, the authors present fluid inclusion microthermometric data which describe the temperatures and compositions of hydrothermal fluids involved in mineralisation and alteration, chert formation and cementation of sediments. They also describe the occurrence, paragenetic and spatial relations of hydrothermal alteration minerals in a traverse across the Rhynie hot-spring system.

1. Mineralisation and alteration

The fault zone defining the western side of the basin in the Rhynie area is called the Rhynie Fault Zone (RFZ), and is marked by a 150-m-wide zone of intense alteration that can be traced along and in the hanging-wall of the fault zone for at least 2 km (Rice *et al.* 2002; Rice & Ashcroft 2004). Hydrothermal mineralisation mainly consists of chert-, quartz- and minor carbonate-bearing breccias and veins with associated pervasive alteration. Two subvertical faults, which cut the RFZ at high angles, are also marked by mineralisation and alteration. Sediments and especially andesitic lavas in the RFZ are pervasively altered to quartz, K-feldspar, calcite, hematite, chlorite and illitic clays, whereas away from the RFZ sediments and lavas are significantly less altered, except where they are adjacent to chert horizons.

Rice & Trewin (1988) showed that the chert beds (henceforth referred to as sinter or siliceous sinter) contain anomalous levels of Au, As, Hg and Sb, which are known to be enriched in some modern hot-spring systems (Barnes & Seward 1997). The RFZ is also enriched in these elements as well as in W and Mo (Rice *et al.* 1995). The highest Au levels occur within the lavas, where they are highly brecciated, and altered to quartz and K-feldspar. As and Au levels display a good correlation, and both appear to be located in arsenian pyrite which displays oscillatory As-zoning with gold in the As-rich zones. Particles of gold have also been noted on the surfaces of quartz and feldspar grains which show evidence of oxidation (Rice *et al.* 1995).

https://doi.org/10.1017/S0263593300000717 Published online by Cambridge University Press

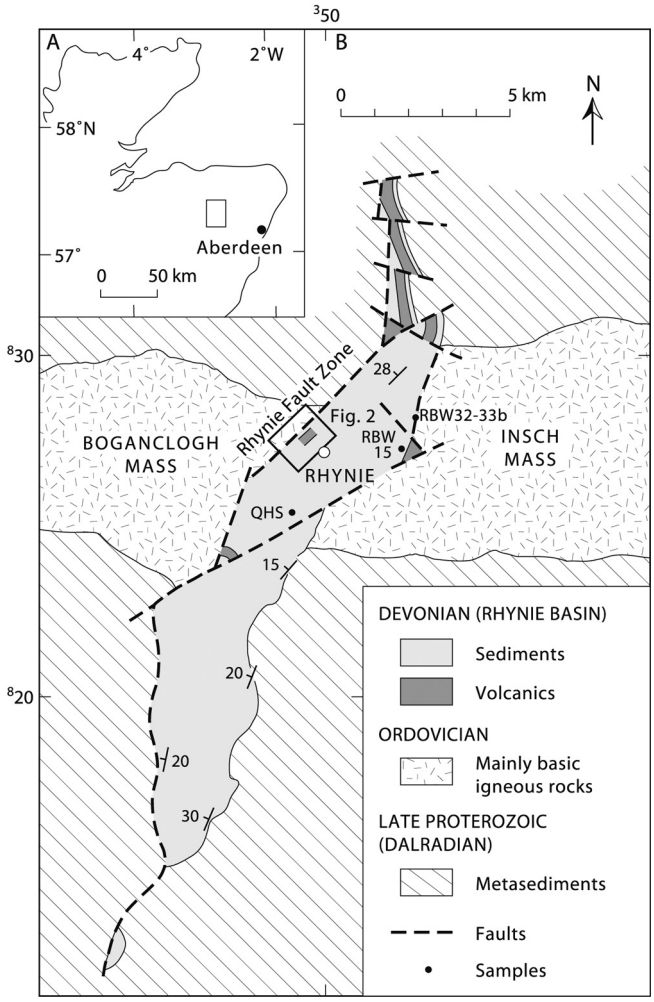

Figure 1 Simplified geological map of the Rhynie basin with sampled localities away from the Rhynie Fault Zone and the location of Figure 2.

The K-feldspar, illitic-chlorite, hematite and pyrite alteration assemblage suggests that the mineralising solutions were near neutral pH, and had low sulphur and oxygen activities (Rice *et al.* 1995). Although hydrothermal alteration is associated with anomalous Mo and W levels, suggesting that late Caledonian granite magmas were implicated in mineralisation, radiometric dating reveals that the granites in the Rhynie area are older than the sinter-bearing sequence (S. Parry, pers. comm.). This indicates that the contemporaneous andesitic volcanism was responsible for the hydrothermal activity.

2. Methods

2.1. Sample location

Because of the poor exposure in the Rhynie region, samples were mainly collected from boreholes, trenches, pits or abandoned quarries (Figs 1, 2). The mineralogy, textural relations and mineral paragenesis were first determined, where possible, from cut and polished blocks and thin sections. Sampling for X-ray powder diffraction (XRPD) was performed on a section across the most intensely altered part of the RFZ, where maximum core was available in order to characterise the alteration assemblages and provide more information on the hydrothermal fluids involved. Sampling for fluid inclusion microthermometry was also concentrated on veins and breccias associated with this part of the system. Veins, sinters and sandstone cements were also sampled away from the RFZ in order to investigate the temperature and composition of the fluids, which may have been circulating within other parts of the basin away from the centre of the hydrothermal system.

2.2. X-ray powder diffraction

X-ray powder diffraction was performed on powdered samples run on a Siemens D5000 diffractometer using cobalt Kα radiation selected by a diffracted beam monochromator. The beam was collimated by fixed one-degree divergence and antiscatter slits, with a receiving slit of 0·6mm. Patterns were recorded from 2 to 75°2θ in steps of 0·02° and counted for one second per step.

Following identification of the minerals present, semi-quantitative analysis of the diffraction data was made by a full pattern scaling normalised (sum=100%) reference intensity ratio (RIR) method (Hillier 2003). Phyllosilicates were quantified simply as dioctahedral or trioctahedral types. Reference patterns were taken from the power diffraction file (PDF), or in the case of the phyllosilicates, from reference minerals, all RIRs were verified on mixtures of pure minerals, and pattern fitting was made using the Siemens/Bruker Diffrac Plus Eva computer software. More detailed identification of the phyllosilicates present was made by analysis of the <2-μm clay size fraction from selected samples. The clay size fraction was separated by timed sedimentation, prepared as oriented specimens on glass slides and examined in the air-dried state, after saturation with ethylene glycol and after heating to 300°C for one hour (Hillier 2003).

2.3. Fluid inclusion microthermometry

Fluid inclusion microthermometric analysis was performed using standard techniques outlined by Shepherd *et al.* (1985). Microthermometric analysis was carried out using a calibrated LINKAM TH-600 stage and measured with the aid of a video screen coupled to a Nikon OPTIPHOT 2-POL microscope. Homogenisation temperature (T_h) measurements were determined using a heating rate of 10°C min^{-1}. Final solid CO_2 melting temperature (T_mCO_2), first ice melting temperature (T_e), final ice melting temperature (T_m), final salt hydrate melting temperature (T_{HH}), partial homogenisation of the CO_2-rich phase temperature (T_mCO_2) and clathrate dissociation temperature (T_mC) measurements were determined using a heating rate of 1°C min^{-1}. Accuracy for measurements below 0°C was ±0·2°C and ±2°C for measurements above 0°C.

Salinities of aqueous inclusions, based on the system H_2O-NaCl, were estimated using the methods of Bodnar (1993) and reported as wt.% NaCl equivalents. Salinities of mixed H_2O-CO_2 inclusions were estimated using the methods of Diamond (1994). Fills were estimated at room temperature by reference to the volumetric charts of Roedder (1984).

T_m measurements for aqueous inclusions that are one-phase (liquid-filled) at room temperature were very difficult to determine accurately. In order to record more accurate reproducible data, these inclusions were rapidly heated to 600°C in order to stretch the mineral host. Once the inclusions cooled back to room temperature, they had often nucleated a vapour phase, because of an increase in the volume of the inclusion, enabling T_m values to be observed more accurately. Vityk & Bodnar (1995) showed that fluid salinities do not change during the re-equilibration of quartz-hosted fluid inclusion volumes, indicating that these measurements are reliable.

3. Sample mineralogy and paragenesis

The samples chosen for the present study consist of quartz ± chert ± K-feldspar ± pyrite veins and breccias from

https://doi.org/10.1017/S0263593300000717 Published online by Cambridge University Press

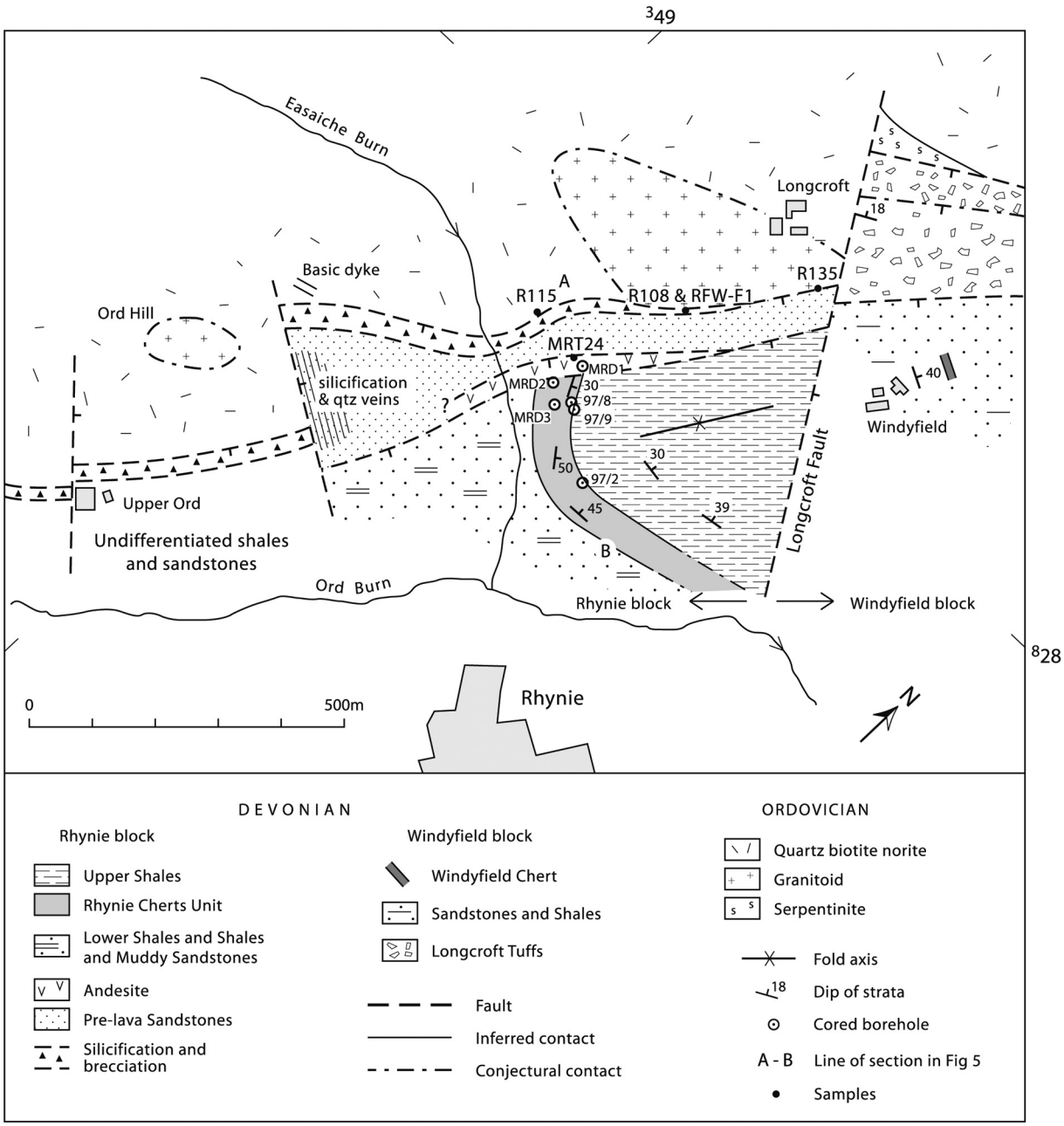

Figure 2 Simplified geological map of the Rhynie area showing sampled localities and the line of cross-section in Figure 5 (adapted from Rice *et al.* 2002).

the RFZ, quartz-calcite veins from the footwall of the RFZ and calcite ± fluorite veins close to the RFZ. Fossil-bearing sinters, also close to the RFZ, and well-cemented sandstones from different parts of the basin were also sampled.

3.1. Mineralisation associated with the RFZ

The mineralised samples from the RFZ are derived from breccia zones and veins ranging in widths from a few millimetres to over 10 cm, and display both replacement and open-space-filling textures. Individual veins display cross-cutting relationships, indicating that mineralisation involved multiple episodes of fracturing and mineral deposition. The wall rock and breccia fragments are highly altered and generally possess a cherty appearance. Quartz, chert, K-feldspar, calcite, pyrite and hematite are the most abundant minerals filling the breccia zones and veins. A detailed examination of the breccia zones and veins reveals a complex paragenesis, a generalisation of which is presented in Figure 3.

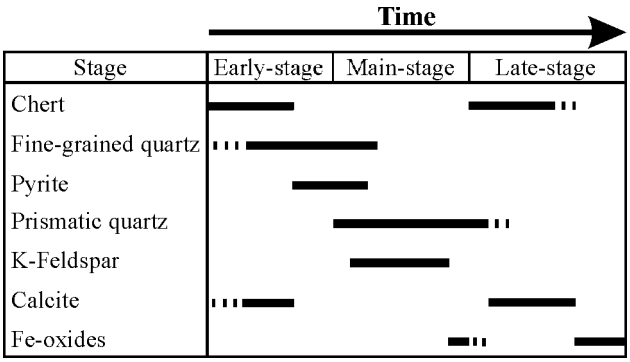

Figure 3 Representative paragenetic sequence of mineralisation associated with the Rhynie Fault Zone.

Early-stage mineral infilling is usually composed of chert or fine-grained quartz (0·25–2 mm). The chert is single- or multiple-layered, cream to brown in colour, microcrystalline

https://doi.org/10.1017/S0263593300000717 Published online by Cambridge University Press

and contains no fluid inclusions suitable for microthermometry. It generally takes the form of a layer up to 3 mm in thickness at the contact between the breccias/veins and the host-rock. This chert also coats rock fragments suspended in the breccias. In veins where chert is absent, the vein/host-rock contact is coated by a thin layer of milky coloured, fine-grained, equigranular quartz. This fine-grained quartz contains very rare fluid inclusions.

A common vein-filling mineral is coarse-grained (5–30 mm), undeformed, transparent and white coloured, prismatic quartz, which contains abundant fluid inclusions. The long axes of these prismatic quartz crystals are orientated at high angles to the vein/host-rock contact. A thin layer of fine-grained equigranular quartz generally occurs at the contact between the main-stage prismatic quartz and the early-stage chert. From these relationships, it can be seen that many of the breccias and veins were deposited in the order chert, fine-grained quartz and prismatic quartz.

Pink coloured K-feldspar crystals commonly occur within some of the wider veins. The feldspar occurs as bands of interstitial crystals within prismatic quartz layers and also as large, irregularly distributed, 5-cm-scale masses (Fig. 4a).

Fine-grained, tens of micrometres to 1-mm, euhedral crystals of pyrite occur within the host-rock adjacent to many breccias and veins. They are usually replaced by iron oxides. Aggregates of pyrite crystals are also enclosed within the early-stage, fine-grained quartz, or more rarely, within the prismatic quartz and K-feldspar.

Calcite is a rare mineral in the RFZ because of dissolution, but there is evidence that it was once a common mineral. Some of the breccias are also filled by large transparent and white, bladed quartz, which has possibly replaced an early, coarse-grained bladed phase of calcite or barite. These blades are now composed of microcrystalline quartz (chert) with minor fine-grained quartz containing very small fluid inclusions (<2 μm) (Fig. 4b, c). Calcite can mainly be found in quartz-calcite veins hosted in norites in the footwall of the RFZ (Fig. 4d). The majority of calcite generally occurs towards the centre of veins, indicating that most of the deposition occurred late in the paragenesis. This phase of calcite is composed of a mosaic of equigranular, coarse-grained (up to 10 mm in diameter) crystals.

Late-stage features include multiple episodes of veinlets filled with chert, vuggy quartz or calcite, which cut many of the breccias and veins. The early vein-fill mineral assemblages are also occasionally mantled by thick, centimetre-scale, layers of banded chert. Hematite occurs as disseminations and stringers mainly within quartz crystals, indicating that it also mainly occurred late in the paragenesis.

3.2. Mineralisation away from the RFZ

Away from the RFZ, centimetre-scale calcite-bearing veins occur cutting sediments and within fault zones elsewhere in the basin. In borehole 97-2, a white sparry, calcite-fluorite vein, with sparse pyrite cuts siliceous sinter-bearing sequences. There are two generations of fluorite within the sample studied, consisting of an early purple fluorite close to the vein margin, and a late green fluorite in the vein centre. The Craig Hall Fault separating basement diorites from Devonian sandstones on the east side of the basin (Rice & Ashcroft 2004) at Bogend contains a 2-cm-wide vein of homogeneous, equigranular, sparry calcite. Abundant fluid inclusions occur hosted within both calcite and fluorite.

3.3. Sandstone cements

The sandstones sampled from the base and middle of the succession consist of fine-grained, well sorted, quartz arenites to sublithic and arkosic arenites. Cements include early quartz overgrowths containing minor fine-grained pyrite followed by late-stage, pore-filling calcite and clays. Both quartz and calcite cements contain fluid inclusions. A sandstone clast (sample MRT24-3) sampled from a breccia within the RFZ contains extensive quartz and K-feldspar cement that also contain fluid inclusions.

3.4. Siliceous sinters

The Rhynie Chert Unit is composed of layers of vuggy to massive chert containing in some cases, preserved plant material. The cherts contain patches of fine-grained quartz (<1 mm in size) which sometimes shows central cavities and often contain relict outlines of early botryoidal chalcedony. Late calcite and fluorite occur as infills to the cavities and also as veins (Fig. 4e). Fluid inclusions are only visible in the fine-grained quartz, calcite and fluorite. Unfortunately, because of the translucent nature of the chert, no fluid inclusions were visible.

4. XRPD results

The results of semi-quantitative analysis by XRPD of a suite of bulk rocks from a traverse across the most intensely altered part of the hot spring system are presented in Table 1 and Figure 5. The main minerals identified in this suite include quartz, K-feldspar, plagioclase feldspar, calcite, chlorite, illitic clays and pyrite. Additionally, some samples contain minor to trace amounts of hematite, fluorite, amphibole and gypsum.

In borehole MRD-1 (Figs 2 & 5) all rocks, especially the andesites, are clearly enriched in K-feldspar, and contain little or no plagioclase. The andesites also contain substantial quantities of quartz, indicating that these rocks have been completely altered to a secondary mineral assemblage. Powder patterns of potassium feldspar obtained from spray-dried samples to ensure a random orientation show that the potassium feldspar matches the composition of pure end-member orthoclase in the PDF. Trioctahedral chlorite appears to be absent from the most intensely altered rocks, and the total phyllosilicate (clay minerals) content is relatively low at around 10 wt.%. Analysis of clay size fractions shows that dioctahedral micaceous/illitic clay is dominant, with little sign of any mixed-layer component. However, a distinct mixed-layer clay mineral is present in the andesites, but it appears to be some form of dioctahedral chlorite/vermiculite, giving a prominent peak at around 14 Å in air-dried samples that fails to expand with glycol treatment and collapses to 12 Å upon heating.

Samples from adjacent borehole MRD-2 also contain K-feldspar at concentrations which appear relatively high when compared to the suite of samples as a whole, but in absolute terms, the concentration of K-feldspar is typically one-third or less than that in the previous borehole (MRD-1). Calcite and pyrite also become prominent in this borehole. Trioctahedral chlorite also appears and the total phyllosilicate content increases dramatically, especially in the andesites where the increased phyllosilicate content is primarily a result of the appearance of abundant mixed-layer illite/smectite. The andesites show a marked decrease in K-feldspar with depth from boreholes MRD-1 to MRD-2, -3 and 97/8, which is balanced by a rise in mixed-layer illite/smectite. All common primary minerals in the andesites are replaced by secondary minerals. Analysis of the clay-sized fraction separated from an andesite in this zone shows that the mixed-layer illite/smectite is an ordered variety with an expandability (percentage of swelling layers) of approximately 15% (Fig. 6).

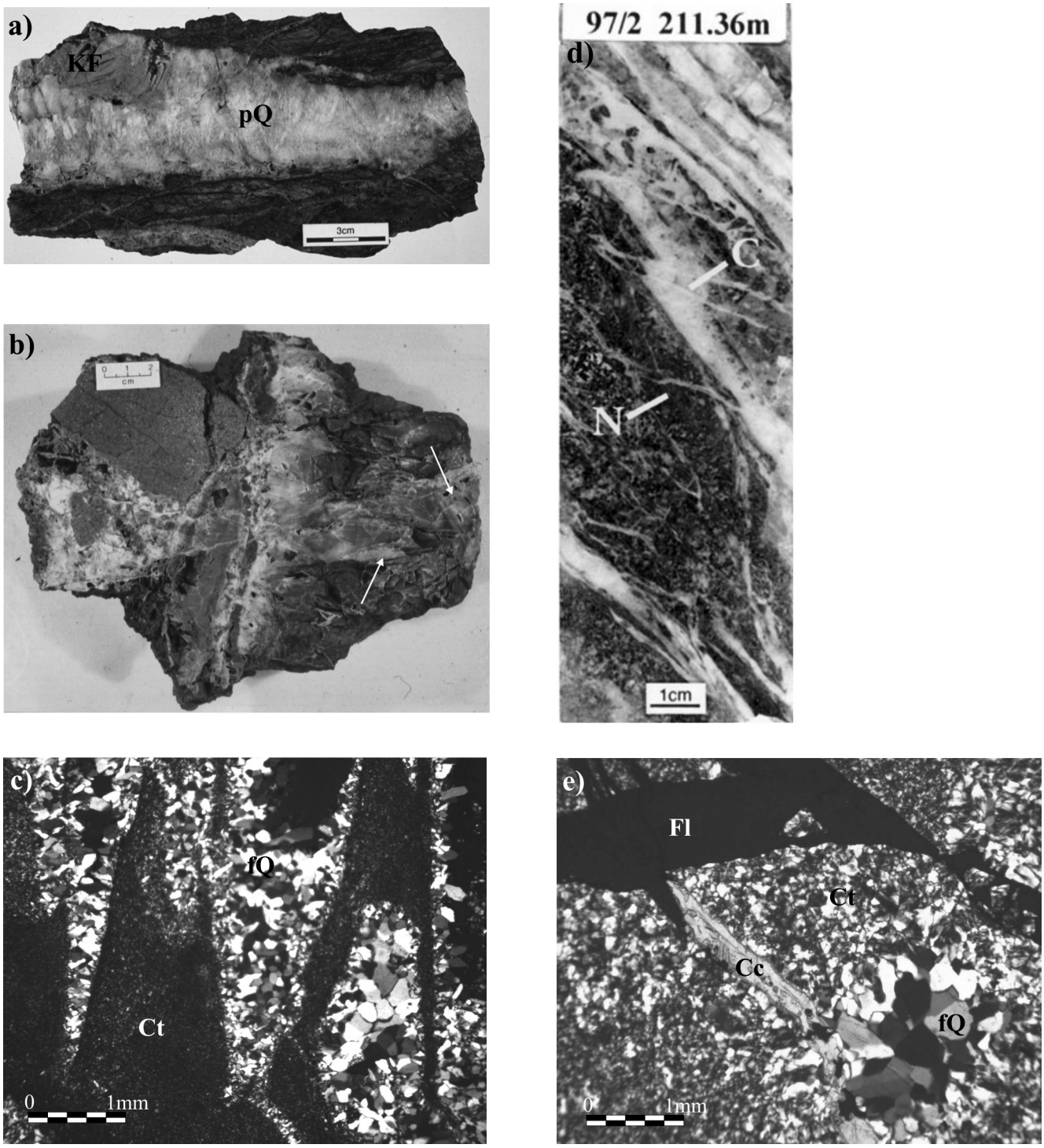

Figure 4 Photographs showing: (a) a chert-hosted vein filled with K-feldspar (KF) and prismatic quartz (pQ) from the Rhynie Fault Zone (RFZ) (sample: R135); (b) a sandstone breccia filled by bladed quartz (arrowed), probably pseudomorphing bladed calcite or barite from the RFZ (sample: MRT24); (c) a transmitted light photograph of microcrystalline quartz (Ct), pseudomorphing bladed calcite and late-stage, fine-grained quartz (fQ) which contain the only fluid inclusions suitable for microthermometry in this sample (sample: MRT24-1); (d) multiple quartz-calcite (C) veins cutting strongly altered quartz-biotite norite (N) of the Boganclough intrusion in the footwall of the RFZ (sample: 97-2 211·4 m); and (e) transmitted light photograph of fossil-bearing chert (Ct) with areas of fine-grained vuggy quartz (fQ) cut by calcite- (Cc) and fluorite- (Fl) filled veins (sample: 97/2 50·3 m). The fluid inclusions chosen for microthermometry were those found in the vuggy quartz (see text).

With the exception of the andesites, the samples taken from the remaining boreholes MRD3, 97/2, 97/8 and 97/9 are from the chert-bearing seqeunces (Fig. 5). These samples all show very similar assemblages of quartz, K-feldspar, plagioclase, calcite, chlorite, illitic clays (mixtures of well-crystallised micas and mixed layer illite/smectite), and minor but sporadic occurrences of pyrite. Broadly speaking, this assemblage is similar to those which characterise the sedimentary rocks elsewhere in the Orcadian Basin (Hillier & Clayton 1989; Hillier 1993). The parental rocks here are dominated by sediments rather than andesite, and from thin-section studies, most of the quartz and feldspars are of detrital rather than hydrothermal origin. The well-crystallised micas identified by XRPD are probably detrital muscovite and biotite. The main secondary minerals are chlorite, illite/smectite and calcite.

https://doi.org/10.1017/S0263593300000717 Published online by Cambridge University Press

Table 1 Semi-quantitative mineralogical composition (wt.%) from X-ray powder diffraction analysis of rock samples from the Rhynie traverse. Other minerals identified include: (A) amphibole; (F) fluorite; (G) gypsum and (H) hematite.

Sample ID	Lithology	Quartz	K-spar	Plagioclase	Calcite	Chlorite	Illite+IS	Pyrite	Other
MRD1/2-4	Andesite	44·5	42·3	5·8	–	–	7·5*	–	
MRD1/10-12	Andesite	37·8	46·5	2·8	–	–	12·9*	–	
MRD1/20-22	Andesite	49·5	41·8	–	–	–	8·7*	–	
MRD1/34-36	Sandstone	73·3	21·3	–	–	–	5·4	–	
MRD1/48-50	Sandstone	72·6	16·4	–	–	–	10·9	–	
MRD2/9·0	Tuff sst	75·3	10·9	1·0	–	–	12·7	–	
MRD2/18.5-20·5	Andesite	40·5	12·4	5·2	3·9	8·8	26·4	2·7	
MRD2/30·5-32·5	Andesite	29·5	13·7	0·9	10·9	5·0	35·4	4·4	
MRD2/40·5-42·5	Andesite	25·3	12·3	7·0	11·1	9·5	32·3	2·6	
MRD2/48·5-50·5	Andesite	27·3	13·1	–	7·6	7·9	40·6	3·6	
MRD3/10·2	Shale and siltstone	25·1	7·1	21·7	0·9	19·0	26·3	–	
MRD3/20·25	Shale and siltstone	15·6	11·9	17·7	16·0	16·1	22·8	–	
MRD3/29·25	Shale and siltstone	30·5	3·8	5·3	37·7	9·7	10·1	2·7	
MRD3/48-50·15	Andesite	21·7	8·6	–	10·3	10·2	45·4	3·8	
97/8/11	Sandstone	54·4	8·9	20·6	–	6·9	9·3	–	
97/8/23	Shale	15·2	6·4	19·4	12·5	24·1	22·4	–	
97/8/32	Mudstone	21·7	4·2	9·1	3·9	27·0	34·0	–	
97/8/44	Mudstone	35·2	8·4	8·1	19·0	11·9	16·4	0·8	
97/8/51·5	Andesite	3·9	5·4	20·1	5·4	–	55·7	–	9·5 (H)
97/9/3·6	Chert	94·5	0·9	–	–	–	4·6	–	
97/9/12	Shale	24·9	5·3	3·1	16·1	19·2	29·4	2·0	
97/9/21	Siltstone	38·2	10·0	8·1	–	19·8	23·9	–	
97/9/33	Shale	35·6	9·1	1·8	8·3	18·6	26·5	–	
97/9/40	Shale	19·5	6·2	16·0	20·9	18·5	18·8	–	
97/9/52·9	Shale	20·6	6·9	12·3	15·9	18·2	22·3	3·8	
97/2/14	Chert	92·1	1·9	–	–	–	3·5	0·9	1·6 (F)
97/2/19·5	Mudstone	39·6	6·2	5·1	–	12·8	33·0	1·7	1·5 (G)
97/2/44	Shale	34·1	9·1	8·2	7·0	11·9	29·6	–	
97/2/71	Shale	21·9	12·0	15·5	18·3	13·4	14·4	4·5	
97/2/90	Shale	29·7	9·7	14·2	15·0	9·5	21·9	–	
97/2/110	Shale/silt	32·6	3·3	8·2	16·2	15·9	23·9	–	
97/2/130	Mudstone	30·0	3·8	11·5	19·2	4·5	26·2	–	4·8 (H)
97/2/150	Shale	24·4	6·2	11·4	10·4	19·8	27·8	–	
97/2/162	Shale	33·5	1·4	7·8	12·8	7·8	33·7	2·9	
97/2/175	Shale/silt	33·2	8·8	6·5	3·0	22·7	25·9	–	
97/2/190	Sandstone	55·5	5·5	13·2	5·7	3·0	17·0	–	
97/2/198	Sandstone	50·9	5·5	12·0	6·1	6·6	18·9	–	
97/2/207·8	Sandstone	47·8	9·3	6·3		9·6	27·1	–	
97/2/219·7	Basic igneous	12·6	4·1	14·4	12·9	42·0	10·1	–	3·9 (A)
97/2/232	Basic igneous	14·8	3·1	17·1	17·8	33·0	8·9	–	5·3 (A)

*These samples also contain a dioctahedral mixed-layer chlorite mineral, probably a mixed-layer chlorite-vermiculite. Note that values are reported to one decimal place both because some minerals are detected at concentrations below 1 wt.%, and because the method of analysis normalises the results to 100 wt.%. However, this does not imply that the method used is accurate or precise at this level: (K-spar) K-feldspar; (sst) sandstones and (I/S) illite/smectite. Sample locations are shown in Figures 2 and 5.

5. Fluid inclusion results

5.1. Fluid inclusion petrography

Petrographic examination reveals that fluid inclusions hosted within quartz, calcite, dolomite and fluorite occur in primary, pseudosecondary and secondary settings according to the criteria of Roedder (1984). These inclusions can be further subdivided into three main types based on the number of phases present at room temperature:

Type 1. At room temperature, these inclusions are one-phase (liquid-filled). They occur in secondary settings in most of the samples and in primary settings within the silicified sinter samples. In secondary settings, these inclusions are typically less than 5 μm in diameter and possess flattened morphologies. The primary type 1 inclusions in the siliceous sinter samples (Fig. 7a) possess negative or sub-negative crystal shape morphologies, and range in size from <2 to 8 μm.

Type 2. At room temperature, these inclusions are two-phase (liquid- and vapour-filled) and are by far the most abundant type of inclusion in all the samples. They occur within primary, pseudosecondary and secondary settings in most of the samples (Fig. 7b). Primary and pseudosecondary

https://doi.org/10.1017/S0263593300000717 Published online by Cambridge University Press

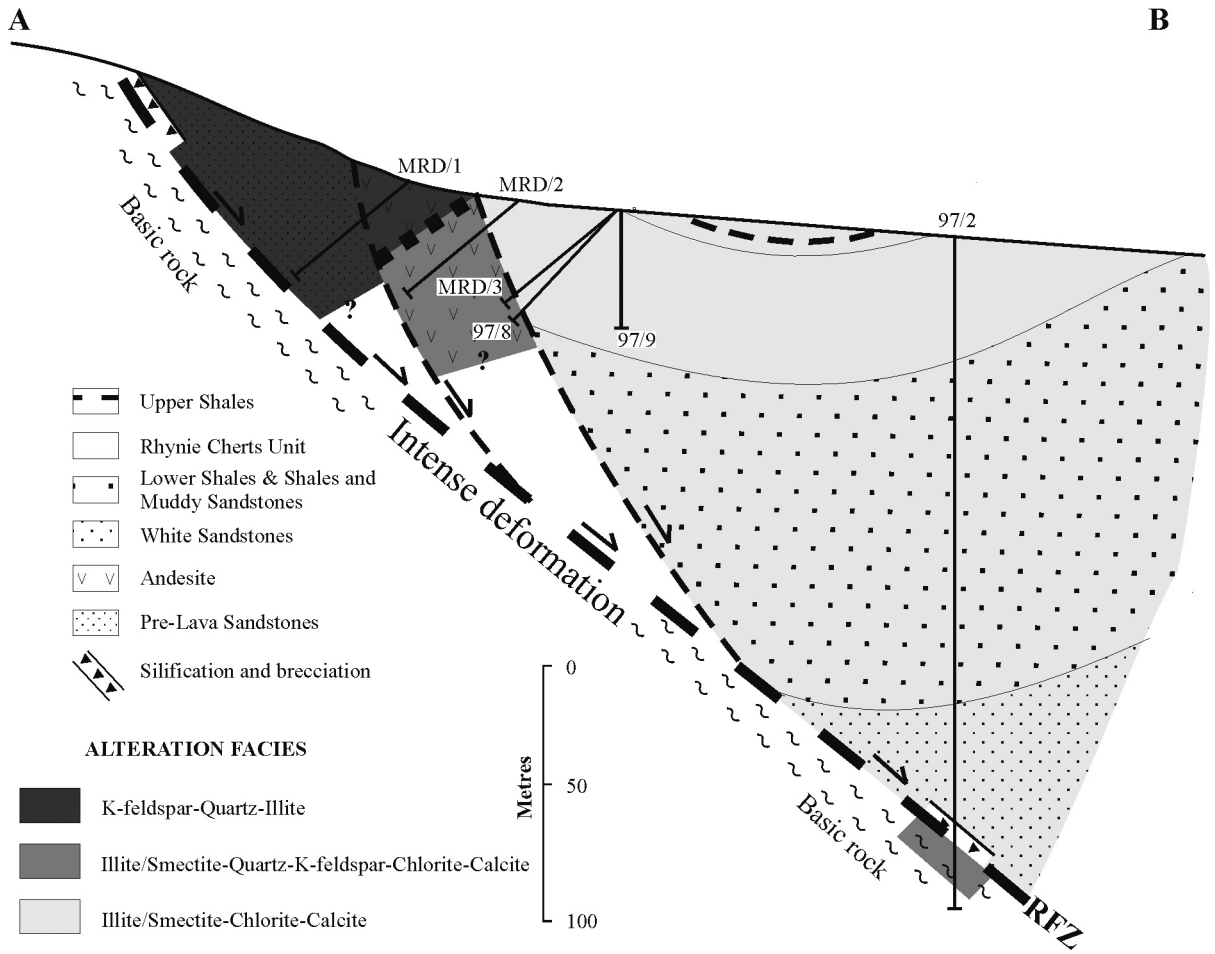

Figure 5 Diagrammatic cross-section of the Rhynie Fault Zone showing the variation in hydrothermal alteration facies, as indicated from X-ray powder diffraction analysis. Geology from Rice *et al.* (2002).

inclusions hosted within quartz generally possess negative or sub-negative crystal shape morphologies, and range in size from 2 to 25 μm. Primary and pseudosecondary inclusions hosted within calcite, dolomite and fluorite possess more irregular or sub-negative crystal shape morphologies, and are generally less than 10 μm in size. Type 2 inclusions within secondary settings typically possess more flattened morphologies and are generally smaller in size than primary and pseudosecondary inclusions in the same mineral host. The degrees of fill at room temperature range from 0·80 to 0·97.

Type 3. At room temperature, these inclusions are three-phase (filled by a vapour phase and two separate liquid phases). They are extremely rare (accounting for less than 1% of the observed inclusions in all the samples), and only occur within quartz from samples R115B and R108E-2 (Fig. 7c, d). They typically possess negative, sub-negative crystal shape or irregular morphologies and are relatively large in size ranging from 25 to 70 μm in diameter.

5.2 Fluid inclusion microthermometric results

Microthermometric data collected from selected fluid inclusions are presented in Table 2 and Figures 8–12. Based on spatial relationships and mineralogy, the breccias and veins can be divided into quartz ± K-feldspar ± calcite veins and breccias which occur within the RFZ, quartz-calcite veins which occur in the footwall of the RFZ, and calcite ± fluorite veins which occur outside the RFZ.

5.2.1. Breccias, veins and cements from the RFZ. The fluid inclusions within the breccias, veins and cements (sample MRT24-3) from the RFZ show overlapping microthermometric characteristics. T_h values of type 2 primary and secondary inclusions which are hosted within quartz and K-feldspars display a similar temperature range of between 84 and 360 °C, with most of the values in the 200 to 230 °C range (Figs 8–12). T_m values of primary inclusions hosted within breccias and veins are in the range of −1·7 to 0 °C, indicating low salinities of between <0·2 and 2·7 wt.% NaCl eq. In contrast, T_m values of primary inclusions hosted within cement from a sandstone clast (sample MRT24-3) range from −5·4 to −0·8, indicating slightly higher salinities of between 1·4 and 8·4 wt.% NaCl eq. Some of the higher salinity values recorded from the RFZ may reflect dissolved CO_2 as evidenced by the presence of calcite (Hedenquist & Henley 1985). T_e values were only observed in a small number of inclusions because of the small size and low salinity of most of the inclusions. T_e values of quartz- and K-feldspar-hosted inclusions range from −46 and −29 °C, suggesting that NaCl, $FeCl_2$ and $MgCl_2$ dominate the salts present (Shepherd *et al.* 1985). Primary late-stage calcite-hosted type 2 inclusions yield slightly lower T_h values, ranging from 91 to 208 °C (average = 142 °C). None of the fluid inclusions examined in the present study display good evidence for boiling.

T_mCO_2 values of the rare type 3 quartz-hosted primary inclusions range from −57·1 to −56·8 °C, indicating the dominance of CO_2. T_hCO_2 values of these inclusions range from 16·0 to 19·2 °C, with homogenisation always occurring by bubble point homogenisation. T_mC values range from 6·4 to 8·3 °C, equating to salinities in the range of 3·5 to 6·6 wt.% NaCl eq. (Diamond 1994). The presence of additional volatiles within the carbonic phase, as suggested from T_mCO_2 values

https://doi.org/10.1017/S0263593300000717 Published online by Cambridge University Press

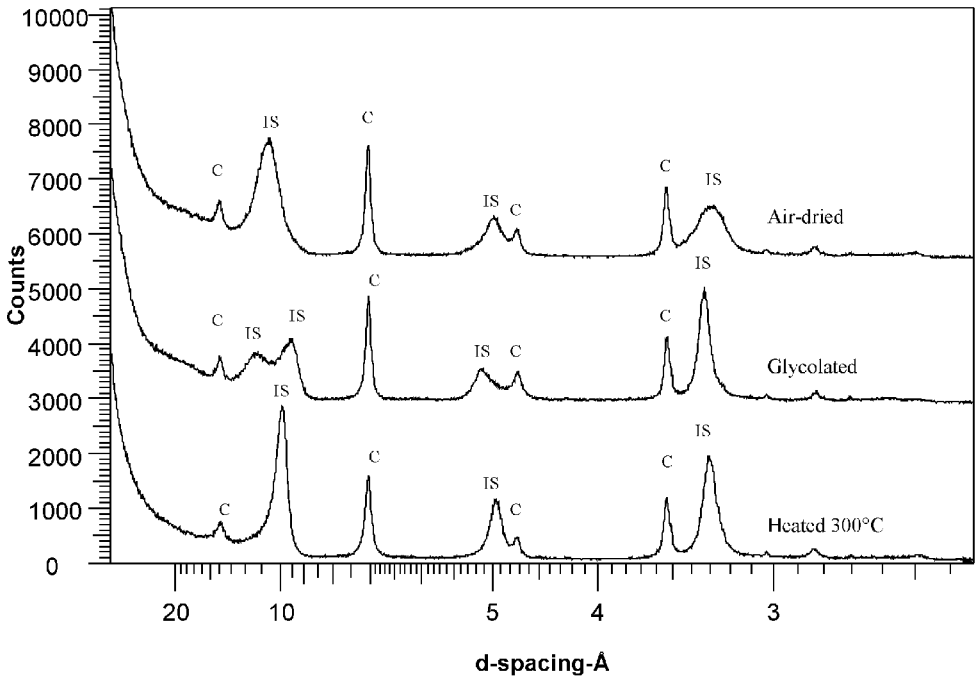

Figure 6 X-ray powder diffraction patterns of the <2-μm clay sized fraction separated from a sample of andesite (MRD1/20-22) showing that the sample is dominated by a mixed-layer illite/smectite (IS) with approximately 15% expandable layers, together with a moderate amount of trioctahedral chlorite (C). Note that the patterns are offset vertically for clarity.

lower than the melting point of pure CO_2 ($-56{\cdot}6$°C), means that the salinity estimates are only minimum values (Diamond 1994). The total homogenisation temperatures of type 3 primary inclusions are variable with values ranging from 245 to 432°C (average=342°C) by bubble point homogenisation.

5.2.2. Veins in the footwall of the RFZ. T_h values of primary type 2 inclusions hosted within the early-stage quartz in a quartz-calcite vein in the footwall of the RFZ range from 142 to 240°C (average=179°C). T_m values range from $-0{\cdot}6$ to $-1{\cdot}1$°C, equating to low salinities in the range of 1·1 to 1·9 wt.% NaCl eq. T_h values of primary type 2 inclusions hosted within the late-stage calcite range from 84 to 152°C (average=128°C). T_m values range from $-3{\cdot}2$ to $-0{\cdot}1$°C, equating to slightly higher salinities of between 0·2 and 5·3 wt.% NaCl eq.

5.2.3. Calcite-fluorite veins and quartz-calcite sandstone cements away from the RFZ. T_h values of primary type 2 inclusions from the calcite-fluorite veins and quartz-calcite cements in sandstones from areas away from the RFZ range from 57 to 161°C, with most of the values in the 110–140°C range (Figs 8, 12). T_m values are very variable, ranging from $-14{\cdot}1$ to 0°C (Fig. 9), which indicates salinities from <0·2 to 17·9 wt.% NaCl eq. Cathodoluminescence and transmitted light petrography reveals the vein-filling calcite within the calcite-fluorite veins is homogeneous, indicating that the inclusions with variable salinities are hosted within the same mineral phase and were not trapped at significantly different times. The most likely explanation for this trend is that mixing of a moderate–high salinity (~15–10 wt.% NaCl eq.), low temperature fluid with a dilute fluid (~0–5 wt.% NaCl eq.) of a similar temperature occurred during vein formation (Fig. 9). The wide range of T_h values of the calcite-hosted inclusions is also probably a product of fluid mixing.

T_e values of primary type 2 calcite and fluorite-hosted fluid inclusions range from $-58{\cdot}4$ to $-41{\cdot}8$°C, suggesting that NaCl and $CaCl_2$ dominated the salts present in solution (Shepherd *et al.* 1985). In some of the larger, higher salinity, calcite-hosted, type 2 primary inclusions, hydrates formed up on freezing. These hydrate minerals, which were probably hydrohalite, dissolve at temperatures between $-26{\cdot}8$ and $-23{\cdot}3$°C. According to the NaCl-$CaCl_2$-H_2O diagram of Oakes *et al.* (1990), T_m and T_{HH} values in this range correspond to molar Ca:Na ratios of approximately 1. Primary, type 2 fluorite-hosted inclusions yield relatively low T_h (87·6–110·3°C) and low T_m ($-11{\cdot}6$ to $-10{\cdot}4$°C) values, similar to the higher salinity calcite-hosted inclusions in the same vein.

5.2.4. Siliceous sinters. All primary inclusions hosted within quartz from the siliceous sinters are type 1 (one-phase, aqueous liquid-filled) at room temperature, indicating that they were entrapped at temperatures below 40–50°C (Goldstein 2001). T_m values range from $-2{\cdot}1$ to 0°C, with most of the values above $-0{\cdot}5$°C (Fig. 10). These values indicate that the inclusions are filled with a dilute aqueous solution with the large majority of salinities less than 1 wt.% NaCl eq. T_h values of secondary type 2 inclusions range from 112 to 155°C, and T_m values range from $-6{\cdot}5$ to $-0{\cdot}2$ °C (Fig. 10), which corresponds to salinities in the range of 9·9 to 0·4 wt.% NaCl eq.

6. Discussion

6.1. Temperatures and compositions of hydrothermal fluids

Fluid inclusion microthermometry has revealed that hydrothermal fluids with variable compositions and temperatures were involved in the formation of breccias and veins from the RFZ, veins away from the RFZ, the siliceous sinters, and cements in sandstones (Figs 11 & 12). The breccias and veins within the RFZ formed from low- to moderate-temperature, low-salinity fluids, whereas the veins and cements away from the RFZ formed from low-temperature, low- to high-salinity fluids. The cements within the siliceous sinters formed from low-temperature, low-salinity fluids.

https://doi.org/10.1017/S0263593300000717 Published online by Cambridge University Press

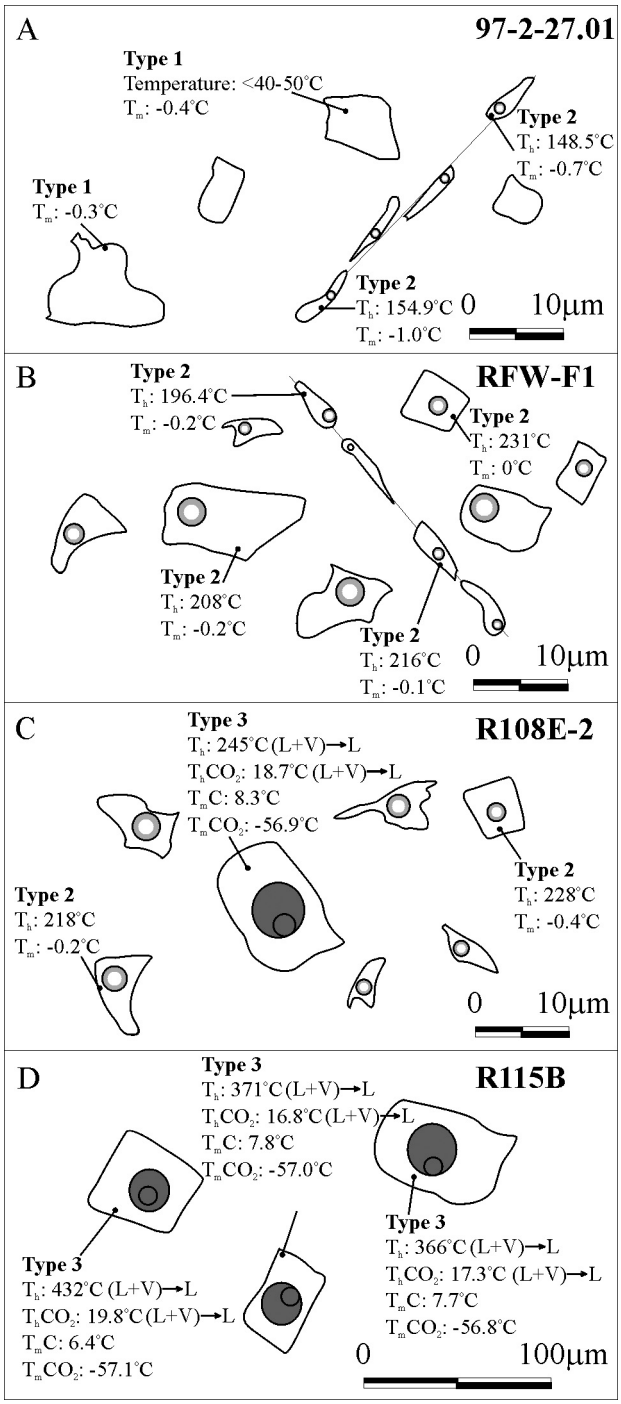

Figure 7 Representative drawing of fluid inclusion assemblages observed within quartz: (a) Primary type 1 (one-phase, liquid-filled) inclusions and secondary type 2 (two-phase, liquid- and vapour-filled) within sample 97-2-27.01. (b) Primary and secondary type 2 inclusions within sample RFW-F1. (c) Primary type 3 (three-phase, filled by a vapour phase and two separate liquid phases) and primary type 2 (two-phase, liquid- and vapour-filled) inclusions within sample R108E-2. (d) Primary type 3 (three-phase, filled by a vapour phase and two separate liquid phases) inclusions within sample R115B. Fluid inclusions from different depths were projected into the plane of the drawing.

6.1.1. Siliceous sinters. The low-temperature (<40–50°C) and low-salinity aqueous composition of the primary inclusions hosted in vuggy quartz within the sinters are typical of near-surface meteoric waters (Goldstein 2001). The low temperature of precipitation suggests that the vuggy quartz was precipitated at very shallow levels soon after deposition of the sinters. The bulk $\delta^{18}O$ composition of the cherty matrix indicates that it formed at temperatures of between 90 and 120°C (Rice *et al.* 1995). However, the noble gas composition of water within the fluid inclusions indicates that the mineralising fluids had interacted with sediments (Rice *et al.* 1995), which would make any temperature estimates from $\delta^{18}O$ compositions suspect.

6.1.2. Hot spring feeder zone. The hydrothermal fluids that fed the hot springs were also responsible for mineralisation at depth within the RFZ. These mainly involved moderate- to high-temperature, low-salinity, aqueous fluids with a minor involvement of high-temperature, low- to moderate-salinity, H_2O-CO_2 fluids.

The salinities of the type 2 primary inclusions hosted in the quartz ± K-feldspar ± calcite veins from the RFZ and the quartz-calcite veins in the footwall of the RFZ are almost identical to the type 1 primary inclusions in quartz from the sinters (Fig. 11). This suggests that these fluids had also originated from surface-derived meteoric waters which had been heated to moderate- to high-temperatures. This interpretation is supported by the $\delta^{18}O$ composition of hydrothermally altered rocks, which indicate that the hydrothermal system along the RFZ was dominated by low-salinity meteoric waters (Rice *et al.* 1995). Minerals containing this type of fluid only occur within breccias and veins associated with the RFZ, indicating that the migration of this fluid was strongly controlled by the RFZ. Furthermore, the recognition of this fluid group in the basic igneous basement rocks in the footwall of the RFZ indicates that it probably migrated along the RFZ and penetrated the basement. This is in agreement with the $\delta^{34}S$ composition of pyrite and the $^{87}Sr/^{86}Sr$ composition of the calcite from veins associated with the RFZ, which demonstrates that the mineralising fluids had interacted with basement lithologies (Rice *et al.* 1995).

The presence of adularia, banded chert and bladed quartz, if pseudomorphing original bladed calcite, all suggest that the fluids had boiled (Browne 1978; Fournier 1985; Simeone & Simmons 1999; Simon *et al.* 1999; Etoh *et al.* 2002). In addition to the mineralogical and textural evidence for boiling, the high Kr/Ar ratios of waters extracted from fluid inclusions in sinters also suggest boiling at the time of mineral deposition (Rice *et al.* 1995). The adularia, banded chert and bladed calcite would have been deposited when boiling led to gas loss (e.g. CO_2 and H_2S), which triggered a sudden increase in the pH of the fluids (Browne 1978; Simmons & Browne 2000). Adularia is also a good indicator of palaeo-permeability in epithermal deposits (Simmons & Browne 2000; Simpson *et al.* 2001), indicating that the RFZ was permeable and allowed extensive circulation of fluids.

Figure 11 shows that the majority of the primary fluid inclusions hosted within quartz and K-feldspar from veins and breccias associated with the RFZ have very low salinities and T_h values from 91 up to 360°C. A fluid with a temperature of 360°C and this composition would boil at depths of less than 1·4 km under hydrostatic conditions (Haas 1971).

T_h values are only a minimum estimate of the temperature at which an inclusion is entrapped (T_t). The difference between T_h and T_t is mainly dependent on the ambient pressure at the time of trapping. The available geological evidence [e.g. vuggy textures, banded chert, Au content, alteration minerals (see below) and evidence for boiling] suggests that mineralisation in the Rhynie area is epithermal in character, and thus, occurred at shallow depths, close to the palaeosurface. Therefore, it is reasonable to assume that the primary inclusions were entrapped at low pressures, and consequently, the T_h values are very close to the actual temperatures of the mineralising fluids. If the fluids were boiling then $T_h = T_t$.

The origin of the CO_2-bearing fluid inclusions within some of the quartz from the RFZ is uncertain. This fluid is

https://doi.org/10.1017/S0263593300000717 Published online by Cambridge University Press

Table 2 Fluid inclusion microthermometric data: T_mCO_2 represents the temperature of final solid CO_2 melting; T_e represents the temperature of first ice melting; T_{HH} represents the temperature of final dissolution of salt hydrates; T_m represents temperature of final ice melting with salinities calculated using the regression of Bodnar (1993); T_mC represents the temperature of clathrate dissociation with minimum salinities calculated using the methods of Diamond (1994); T_hCO_2 represents the temperature of partial homogenisation of the CO_2-rich phase (all values of T_hCO_2 occurred by bubble point homogenisation); T_h represents the temperature of homogenisation (all values of T_h occurred by bubble point homogenisation); and No. represents the number of measurements determined. Sample locations are shown in Figures 2 and 5: (RFZ) Rhynie Fault Zone.

Sample No.	Sample description	Host	Timing	Type	T_mCO_2 (°C) (No.)	T_e (°C) (No.)	T_{HH} (C) (No.)	T_m (°C) (No.) (Salinity)	T_mC (°C) (No.)	T_hCO_2 (°C) (No.)	T_h (°C) (No.)
Trench MRT24-1	Quartz-filling sandstone breccia from the RFZ	Fine-grained quartz	Primary	2				− 0·7 to − 0·1 (20) (0·2 to 1·2)			200 to 326 (20)
		Fine-grained quartz	Secondary	2				− 0·2 to − 0·1 (4) (0·2 to 0·4)			120 to 275 (4)
Trench MRT24-2	Quartz-filling sandstone breccia from the RFZ	Fine-grained quartz	Primary	2		− 40 to − 36 (2)		− 0·6 to − 0·1 (22) (0·2 to 1·1)			141 to 360 (23)
		Fine-grained quartz	Secondary	2				− 0·4 (1) (0·7)			210 (1
Trench R108E-1	Quartz-K-feldspar vein from the RFZ	Prismatic quartz	Primary	2		− 40 to − 37 (2)		− 0·6 to − 0·3 (4) (0·5 to 0·7)			208 to 219 (4)
		K-feldspar	Primary	2		− 40 to − 38 (3)		− 1·7 to − 0·3 (8) (0·5 to 2·9)			198 to 261 (8)
Trench R108E-2	Quartz-K-feldspar vein from the RFZ	Prismatic quartz	Primary	2				− 0·4 to − 0·2 (8) (0·4 to 0·7)			111 to 252 (14)
		Prismatic quartz	Primary	3	− 57·0 (1)			− 2·6 (1)	8·3 (1)	18·7 (1)	245 (1)
		Prismatic quartz	Secondary	2				− 0·8 to − 0·4 (15) (0·7 to 1·4)			144 to 241 (17)
Trench RFW-F1	Quartz vein from the RFZ	Prismatic quartz	Primary	2		− 46 to − 41 (2)		− 0·8 to 0 (27) (<0·2 to 1·4)			152 to 251 (27)
		Prismatic quartz	Secondary	2				− 11·6 to − 0·1 (5) (0·2 to 15·6)			118 to 287 (5)
Trench R115B	Quartz-K-feldspar vein from the RFZ	Fine-grained quartz	Primary	3	− 57·1 to − 56·8 (4)			− 6·7 to − 7·4 (4)	6·4 to 7·8 (4)	16·8 to 19·8 (4)	279 to 432 (7)
		Prismatic quartz	Primary	2				− 0·9 to − 0·4 (2) (0·7 to 1·6)			118 to 148 (2)
		Prismatic quartz	Secondary	2				− 1·8 to 0 (6) (<0·2 to 3·1)			97 to 196 (6)
		K-feldspar	Primary	2		− 40 to − 30 (3)		− 0·4 to − 0·1 (5) (0·2 to 0·7)			197 to 250 (5)
Trench R135B	Quartz-K-feldspar vein from the RFZ	Prismatic quartz	Primary	2		− 40 to − 37 (3)		− 0·6 to − 0·1 (13) (0·2 to 1·1)			145 to 223 (13)
		Prismatic quartz	Secondary	2				− 0·7 to 0 (8) (<0·2 to 1·3)			157 to 264 (17)
		K-feldspar	Primary	2		− 44 to − 35 (3)		− 1·7 to − 0·3 (7) (0·5 to 2·9)			195 to 264 (7)

Table 2 *Continued*

Sample No.	Sample description	Host	Timing	Type	T_mCO_2 (°C) (No.)	T_e (°C) (No.)	T_{HH} (C) (No.)	T_m (°C) (No.) (Salinity)	T_mC (°C) (No.)	T_hCO_2 (°C) (No.)	T_h (°C) (No.)
Borehole 97-2 (56·2 m)	Calcite-fluorite vein away from the RFZ	Calcite	Primary	2		− 56 to − 47 (5)	− 27 to − 23 (5)	− 14·1 to − 2·4 (25) (4·0 to 17·9)			57 to 144 (34)
		Purple fluorite	Primary	2		− 58 to − 56 (2)		− 11·6 to − 10·4 (5) (14·4 to 15·6)			88 to 110 (9)
Borehole 97-2 (211·4 m)	Quartz-calcite breccia from the RFZ	Fine-grained quartz	Primary	2		− 44 (1)		− 1·6 to − 0·3 (13) (0·5 to 2·7)			154 to 206 (13)
		Fine-grained quartz	Secondary	2				− 0·2 (1) (0·4)			136 to 144 (2)
		Calcite	Primary	2		− 52 to − 47 (2)		− 2·3 to 0 (25) (<0·2 to 3·9)			90·7 to 208 (25)
		Calcite	Secondary	2				− 1·3 to − 0·5 (3) (0·9 to 2·2)			91 to 156 (6)
Borehole 97-2 (215 m)	Calcite-quartz vein in footwall of the RFZ	Prismatic quartz	Primary	2				− 1·1 to − 0·6 (4) (1·1 to 1·9)			142 to 240 (7)
		Calcite	Primary	2				− 3·2 to − 0·1 (13) (0·2 to 5·3)			84 to 152 (20)
Trench MRT24-3	Cement in sandstone clast from the RFZ	Quartz	Primary	2				− 5·4 to − 0·8 (3) (1·4 to 8·4)			84 to 186 (7)
		Quartz	Secondary	2				− 7·7 to − 6·3 (6) (6·8 to 8·7)			151 to 183 (8)
		K-feldspar	Primary	2				− 2·9 to − 2·4 (2) (4·0 to 4·8)			1745 to 241 (4)
Trench RBW15	Cement in sandstone away from the RFZ	Quartz	Primary	2				− 1·7 to − 0·2 (5) (0·4 to 2·9)			86 to 139 (17)
Exposure QHS	Cement in sandstone away from the RFZ	Quartz	Primary	2				− 13·2 to − 6·6 (7) (10.0 to 17·1)			93 to 122 (7)
		Calcite	Primary	2				− 0·6 to − 0·1 (5) (0·2 to 1·1)			83 to 118 (5)
Trench RBW32-33b	Calcite vein away from the RFZ	Calcite	Primary	2		− 42 to − 48 (5)		− 7·6 to 0 (27) (<0·2 to 11·2)			62 to 161 (32)
		Calcite	Secondary	2				− 1·3 to − 0·5 (3) (0·9 to 2·2)			91 to 156 (6)
Trench R-33b	Siliceous sinter	Quartz	Primary	1				− 0·4 to 0 (3) (<0·2 to 0·7)			
Borehole 97-2 (13·1 m)	Siliceous sinter	Quartz	Primary	1				− 2·1 to − 0·1 (12) (0·2 to 3·6)			
Borehole 97-2 (23·17 m)	Siliceous sinter	Quartz	Primary	1				− 0·8 to − 0·1 (11) (0·2 to 1·4)			
Borehole 97-2 (27·01 m)	Siliceous sinter	Quartz	Primary	1				− 0·4 to − 0·1 (4) (0·2 to 0·7)			
		Quartz	Secondary	2				− 6·5 to − 0·2 (11) (0·2 to 9·9)			112 to 155 (13)

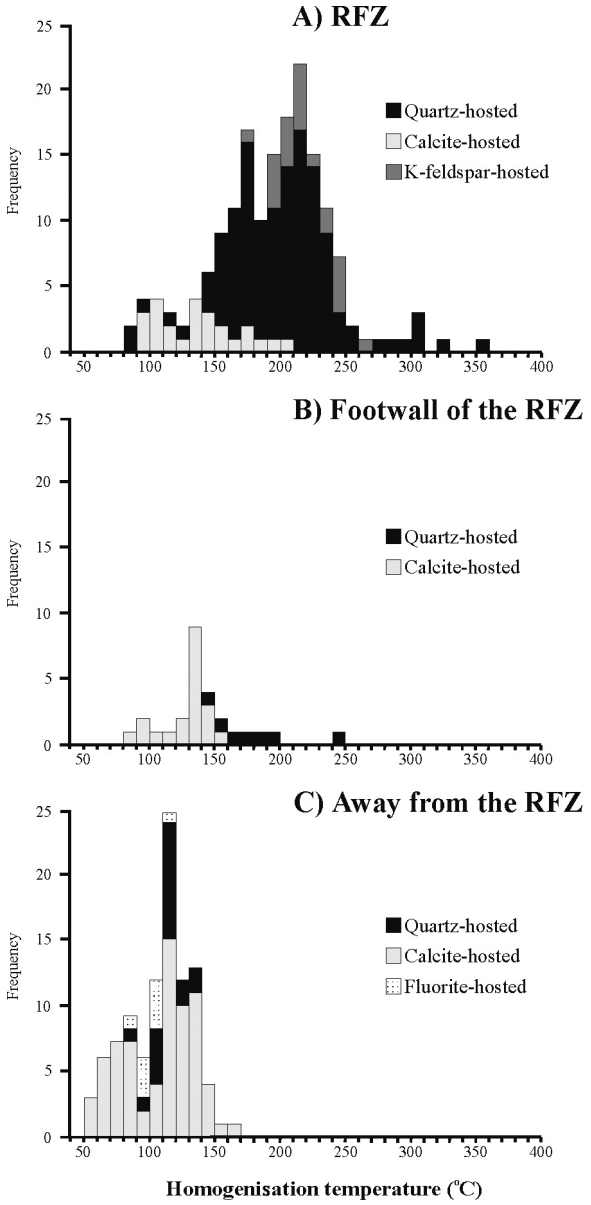

Figure 8 Histograms of homogenisation temperatures of type 2 primary fluid inclusions hosted within quartz, calcite, K-feldspar and fluorite from (a) the Rhynie Fault Zone (RFZ), (b) the footwall of the RFZ and (c) away from the RFZ.

tentatively interpreted to have originated from a magmatic source. Such fluids are implicated in mineralisation in other areas of the British Caledonides (e.g. Alderton 1988; Curtis *et al.* 1993; Wilkinson *et al.* 1999). A magmatic origin for this fluid is also supported by the measured δD and calculated fluid $\delta^{18}O$ of quartz hosting these inclusions (Rice *et al.* 1995).

6.1.3. Basinal brines. Although fluorite is a common vein-fill mineral associated with Caledonian granitoid intrusions in this region (Gallagher 1991), the temperature and composition of the fluids that precipitated the calcite ± fluorite veins and some of the quartz cement away from the RFZ are inconsistent with a magmatic origin. These fluids are different from those responsible for mineralisation along the RFZ and are more consistent with basinal brines (Walderhaug 1994). The variable salinity of calcite-hosted fluid inclusions indicates that mixing of a low temperature saline fluid with a dilute fluid of a similar temperature occurred during the formation of these veins (Fig. 9).

Low-temperature, basinal brines can attain their saline composition through either interaction with evaporitic fluids and/or evaporitic horizons, or through extensive water-rock interactions. Caliche horizons occur in the Rhynie Basin (Trewin & Rice 1992), and there are a number of occurrences of evaporite horizons and replaced evaporite horizons in the sedimentary successions elsewhere in NE Scotland. The Lower Old Red Sandstone rocks in Easter Ross contain evidence for replaced evaporitic gypsum (Parnell 1985), and there are also extensive evaporite horizons in the Permo-Triassic successions of the Moray Firth basin to the north of Rhynie (Coward 1995).

The presence of inclusions with relatively high T_h values and low to moderate salinities from cements in a sandstone clast from the RFZ (sample MDT24-3) indicate that slightly higher temperature brines were involved in cementation before the hot spring activity. In addition, secondary inclusions hosted in quartz from the siliceous sinters and vein-filling quartz from the RFZ yield T_h and salinity values comparable with primary inclusions from the calcite-fluorite veins, suggesting that these more saline fluids postdate the main-stage quartz-K-feldspar-calcite mineralisation. Thus, basinal brines may have entered the RFZ at various times during the development of the Rhynie Basin.

6.2. Comparisons of fluids at Rhynie with other gold-bearing hot-spring systems

The majority of the most recent fossil gold-bearing hot springs occur along the margins of the Pacific. Fluid inclusion studies from deposits in Mexico (Simmons *et al.* 1988), the USA (Norman *et al.* 1991), New Zealand, (Simmons & Browne 1997; Simpson *et al.* 2001), the Philippines (Comsti *et al.* 1990), Indonesia (Simmons & Browne 1990) and Japan (Izawa *et al.* 1990; Shikazono & Nagayama 1993; Scott & Watanabe 1998) all yield T_h values of between 150 and 294°C, with many of the values in the 200–250°C range. These values are very similar to the primary inclusions within quartz-K-feldspar-calcite breccias and veins associated with the RFZ. A small number of these deposits contain fluid inclusions which yield unusually high salinities (Simmons & Browne 1997; Scott & Watanabe 1998). These fluids are believed to have reached such saline compositions by open-system boiling to near dryness, a process that does not appear to be important at Rhynie (Simmons & Browne 1997; Scott & Watanabe 1998).

However, the fluids in the large majority of these more recent deposits have very low salinity (less than 4 wt.% NaCl eq.) aqueous compositions. The composition and temperature of the mineralising fluids in these deposits are very similar to the fluids which formed the hydrothermal alteration along the RFZ at Rhynie. The fluid inclusion results in the present study indicate that the dominant fluid involved in mineralisation associated with the RFZ was a moderate- to high-temperature (T_h 91 to 360°C), low-salinity (0 to 2·9 wt.% NaCl eq.) H_2O-NaCl fluid.

The actively gold-depositing geothermal system at Rotokawa in New Zealand is a good modern analogue in terms of geochemistry for the Rhynie hot-spring system. The fluids involved in this system are dilute chloride meteoric waters which deposited anomalous levels of various heavy metals including Au, As, Sb, W and Hg (Krupp & Seward 1987) which are present in anomalous levels at Rhynie. Drilling in the geothermal system reveals that the fluids reach temperatures of up to 320°C (Krupp & Seward 1987), which is very similar to the temperature estimates of the fluids responsible for mineralisation associated with the RFZ at Rhynie. Wells drilled in other geothermal systems to depths where the temperatures are above 370–400°C encounter little permeability (Fournier 1991). This places a rough upper limit on the temperatures which hydrothermal fluids reach in active hot spring systems.

https://doi.org/10.1017/S0263593300000717 Published online by Cambridge University Press

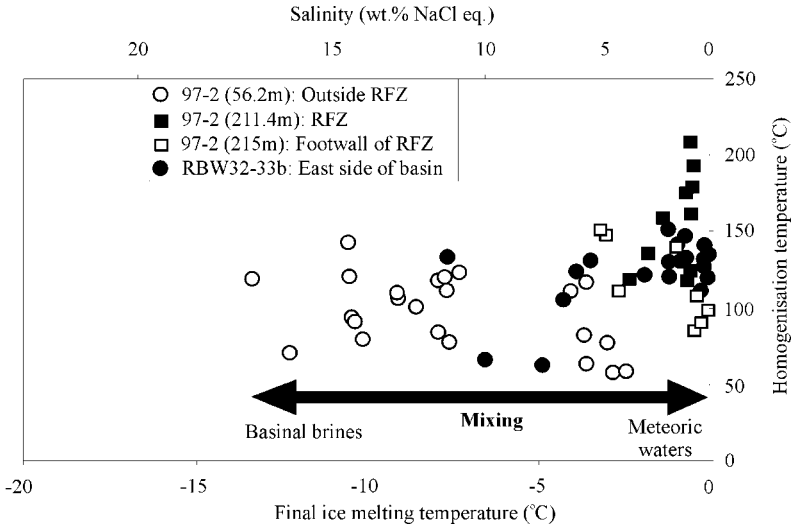

Figure 9 Final ice melting temperature versus homogenisation temperature of calcite-hosted type 2 primary inclusions.

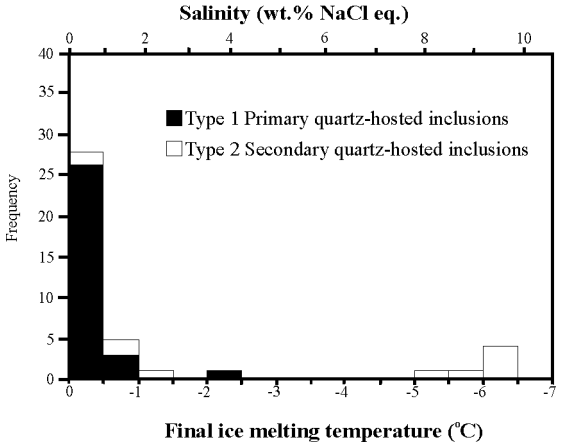

Figure 10 Histogram of final ice melting temperatures of type 1 primary inclusions and type 2 secondary inclusions within quartz from the siliceous sinters.

6.3. Comparisons of alteration assemblages at Rhynie with other gold-bearing hot-spring systems

The XRPD studies have established that the RFZ is characterised at the surface by an alteration facies dominated by K-feldspar and quartz with minor illite that changes with depth to one dominated by mixed-layer illite/smectite and quartz with minor K-feldspar, calcite and chlorite (Fig. 5). In contrast, the chert-bearing sequence away from the RFZ is characterised by a facies of mixed-layer illite/smectite, calcite and chlorite that corresponds to that produced by regional burial of similar sediments elsewhere.

These alteration assemblages associated with the RFZ are typical of epithermal hot-spring systems (Henley & Ellis 1983; Heald *et al.* 1987; White *et al.* 1995). In more recent geothermal systems, the alteration assemblages are good indicators of temperature and depth. The mineral assemblages in the hottest part of geothermal systems are generally dominated by quartz and K-feldspar, with chlorite, mixed-layer illite/smectite and smectite clays occurring towards the edge (Henley & Ellis 1983; Braithwaite & Faure 2002). By analogy with these modern systems, we can interpret the quartz-K-feldspar alteration zone associated with the RFZ as a deep level in the system that has been juxtaposed against shallow levels (i.e. the sinters) by faulting.

Again by analogy with similar systems elsewhere, the K-feldspar-quartz-illite alteration facies formed at temperatures in the 250 to 350°C range (Inoue 1995). Chlorite clays in geothermal systems are generally replaced by illite at temperatures of ~200°C (Henley & Ellis 1983). This suggests that the illite/smectite-quartz-K-feldspar-chlorite-calcite alteration facies formed at temperatures above 200°C (Fig. 13). However, comparison with other hydrothermal occurrences of mixed-layer illite/smectite (Jennings & Thomson 1986; Inoue 1995) suggests that a temperature of between 150 and 200°C is appropriate for the ordered mixed-layer illite/smectite observed in the andesites from this facies. The total range inferred from the alteration facies of 150 to 350°C is similar to the temperatures derived from primary fluid inclusions hosted in K-feldspar and quartz from this zone (T_h=91 to 360°C). By analogy with modern geothermal systems, the temperature range, mineralogy and precious metal content suggests that the K-feldspar-quartz-illite alteration zone formed at shallow levels of less than 500 m (Browne 1978; Henley & Ellis 1983; De Ronde & Blattner 1988; Simmons & Browne 2000).

The temperature inversion indicated by the alteration facies in the RFZ indicates that the bulk of the K-feldspar-quartz-illite facies has been eroded. Given that this contains the highest gold levels and is normally the zone where economic concentrations of gold are to be found, then the ore potential of this system is low unless a portion of the gold-bearing zone has been down faulted to the east.

The intense alteration of the RFZ indicates that it was the main pathway for fluid migration. The dominant fluid type was heated meteoric water that migrated from depth upwards along the RFZ (Fig. 13). The alteration mineral assemblages suggest that the fluids were neutral to weakly alkaline chloride waters (Henley & Ellis 1983).

6.4. Origin, transport and deposition of gold

From the available evidence, it remains uncertain how gold may have been originally introduced into the hot-spring system at Rhynie. However, studies on other gold-bearing hydrothermal systems associated with magmatism have revealed that the metal content is dominantly controlled by metal partitioning between magma and an exsolving fluid rather than scavenging of metals from crustal rocks by surface-derived fluids (Ulrich *et al.* 1999). This suggests that the gold was originally introduced into the hot-spring system at Rhynie during the intrusion of the andesitic magmas. Gold would probably have been transported as bisulphide complexes in such a situation (Giggenbach 1997; Seward & Barnes 1997). There are a number of possible

https://doi.org/10.1017/S0263593300000717 Published online by Cambridge University Press

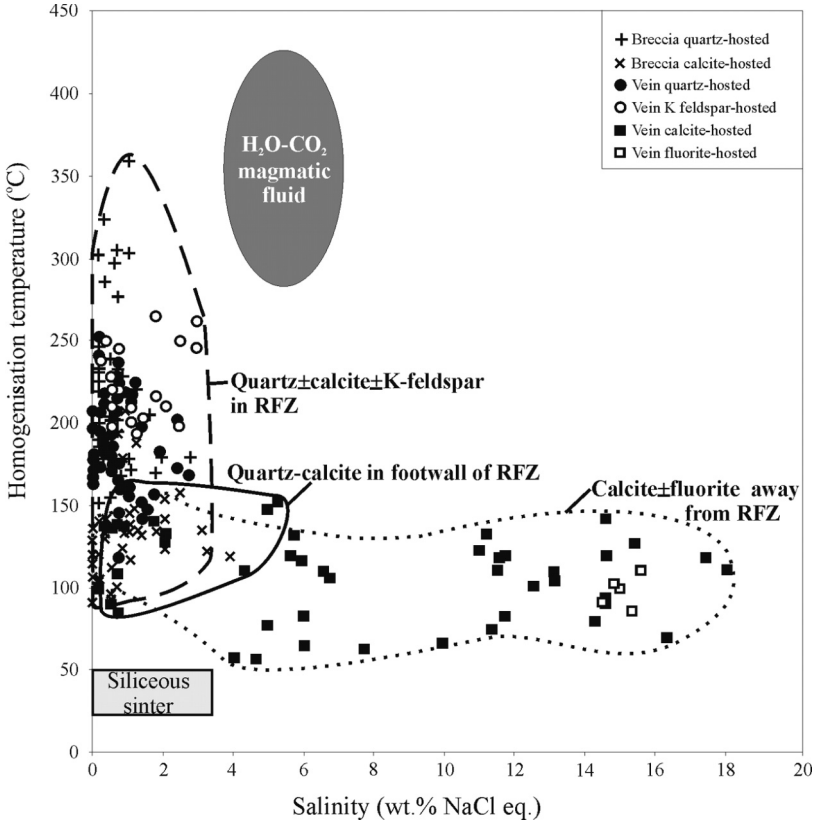

Figure 11 Salinity versus homogenisation temperature of all type 2 primary inclusions hosted within veins and breccias. Fields for type 1 inclusions from siliceous sinters are also shown.

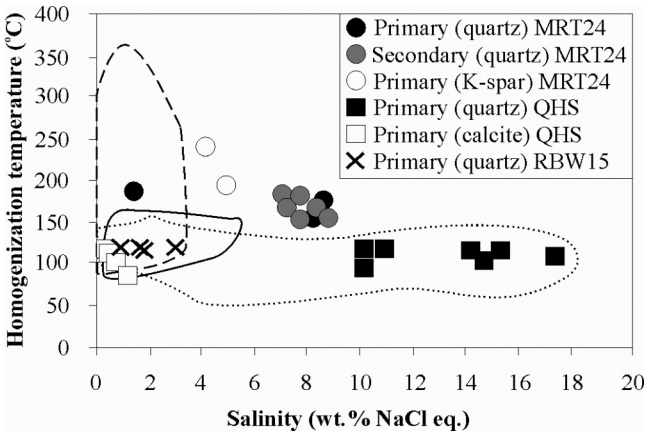

Figure 12 Salinity versus homogenisation temperature of type 2 primary and secondary inclusions hosted within cements in Devonian sandstones. Fluid inclusion host mineral in brackets. Sample MRT24 is a sandstone clast in a quartz-filled breccia from the Rhynie Fault Zone (RFZ). Samples QHS and RBW15 are away from the RFZ. Fields also shown are from the primary inclusions hosted within breccias and veins from Figure 11.

mechanisms which could have caused gold deposition. One possibility is that the reaction between FeO in the andesitic lavas, where the highest gold values occur, and reduced sulphur in the fluids would have destabilised the gold–bisulphide complexes resulting in gold and pyrite precipitation (Rice *et al.* 1995). Another possibility is that boiling caused gold deposition. When the mineralising solutions boiled, gas exsolution (e.g. CO_2 and H_2S) would have triggered a sudden increase in the pH of the fluid resulting in the gold–bisulphide complexes destabilising (Drummond & Ohmoto 1985; Henley 1985). Gold deposition might also have occurred when the gold-bearing solutions rising from depth came into contact with cooler waters close to the surface (Rice *et al.* 1995).

7. Conclusions

The present study has provided important insights into the temperatures and compositions of the hydrothermal fluids responsible for mineralisation, alteration and cemtentation, as well as the occurrence, paragenetic relations and spatial relations of hydrothermal alteration minerals in the Rhynie hot-spring system:

1. There were a number of fluids with different temperatures and compositions involved in mineralisation, alteration and cementation in the Rhynie basin.

2. Quartz ± K-feldspar ± calcite filling breccias and veins associated with the RFZ were mainly precipitated by moderate- to high-temperature (T_h=91–360°C), low-salinity (0–2·9 wt.% NaCl eq.) H_2O-NaCl heated meteoric fluids.

3. A minor input of high-temperature (T_h=280–430°C), moderate-salinity (~4–7 wt.% NaCl eq.) H_2O-CO_2 fluid, probably derived from contemporaneous magmatism, was also involved in mineralisation along the RFZ.

4. Quartz cementation in the siliceous sinters involved low-temperature (<40–50°C), low-salinity (0–3·5 wt.% NaCl eq.) H_2O-NaCl meteoric fluids.

5. Calcite ± fluorite veins outside the RFZ and cementation of the Devonian sediments away from the RFZ involved low temperature (T_h = −57–160°C), low- to high-salinity (0–18 wt.% NaCl eq.) H_2O-NaCl fluids which resemble basinal brines.

6. Hydrothermal alteration facies may be divided into a high-temperature (250–350°C) K-feldspar-quartz-illite facies, a medium-temperature (150–200°C), mixed-1ayer illite/smectite-quartz-K-feldspar-chlorite-calcite facies and a low-temperature (100–150+°C) illite/smectite-chlorite-calcite facies, which have been brought into juxtaposition by faulting.

7. The mineralogy of the alteration facies in the Rhynie hot-spring system and the temperature/composition of the mineralising fluids are comparable with those seen in modern geothermal systems.

https://doi.org/10.1017/S0263593300000717 Published online by Cambridge University Press

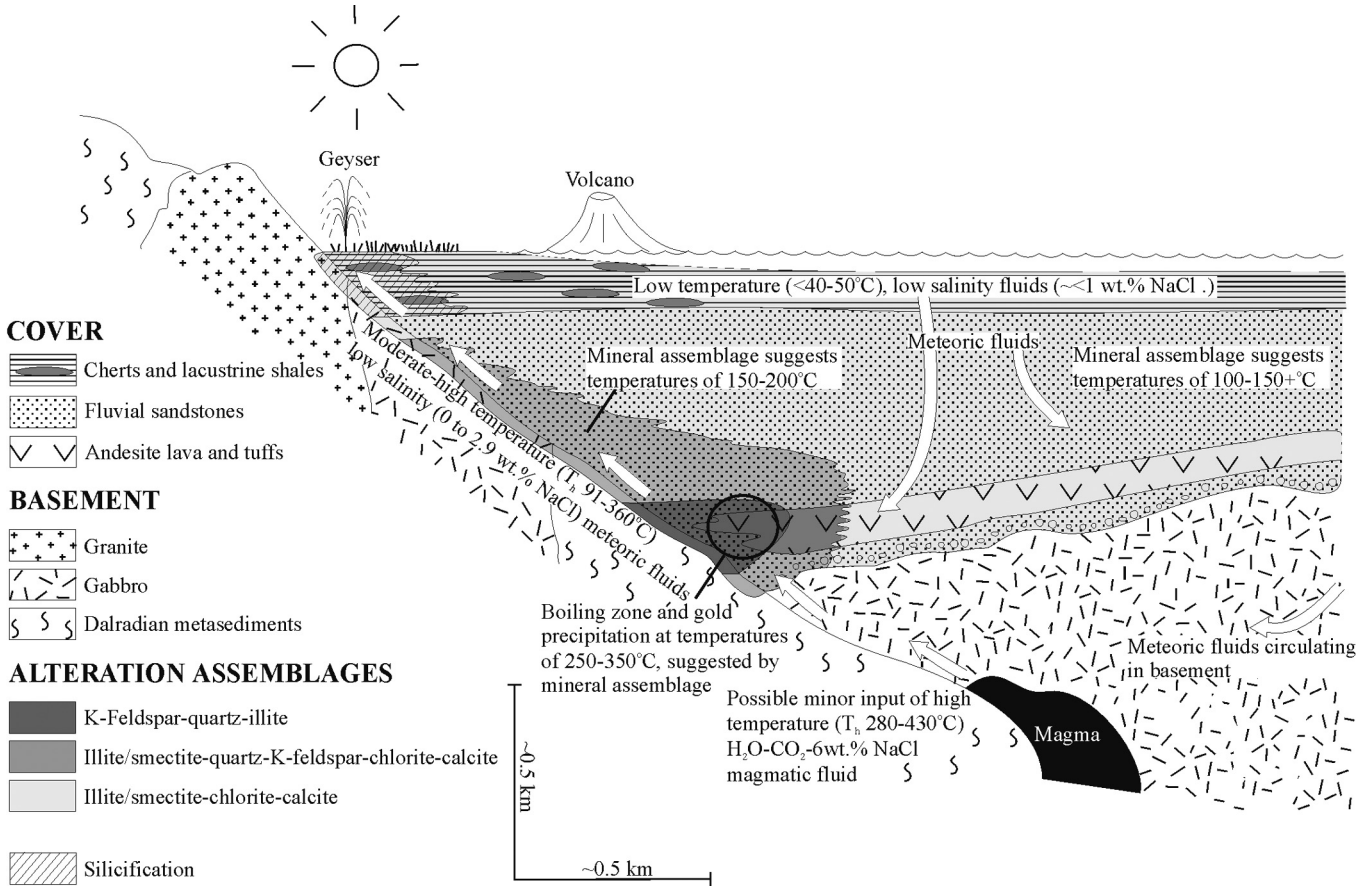

Figure 13 Subsurface reconstruction of the fluids and alteration assemblages in the Rhynie hot-spring system.

8. The bulk of the gold-bearing K-feldspar-quartz-illite zone appears to have been eroded, indicating that the ore potential is low unless a portion of the zone has been preserved by downfaulting.

8. Acknowledgements

T. J. Shepherd, D. A. Banks and J. Naden are thanked for their constructive reviews.

9. References

Alderton, D. H. M. 1988. Ag-Au-Te mineralization in the Ratagain complex, northwest Scotland. *Transactions of the Institution of Mining and Metallurgy (Section B Applied Earth Sciences)* **97**, B171–80.

Barnes, H. L. & Seward, T. M. 1997. Geothermal systems and mercury deposits. *In* Barnes, H. L. (ed.) *The Geochemistry of Hydrothermal Ore Deposits*, 3rd edn, 699–736. Chichester: John Wiley and Sons.

British Geological Survey (BGS) 1993. Alford. Scotland. Sheet 76W. Solid Geology 1:50,000. Nottingham: British Geological Survey.

Bodnar, R. J. 1993. Revised equation and table for determining the freezing point depression of H_2O-NaCl solutions. *Geochimica et Cosmochimica Acta* **57**, 683–4.

Braithwaite, R. L. & Faure, K. 2002. The Waihi epithermal gold-silver-base metal sulfide-quartz vein system, New Zealand: temperature and salinity controls on electrum and sulfide deposition. *Economic Geology* **97**, 269–90.

Browne, P. R. L. 1978. Hydrothermal alteration in active geothermal fields. *Annual Reviews in Earth and Planetary Sciences* **6**, 229–50.

Busrewil, M. T., Pankhurst, R. J. & Wadsworth, W. J. 1973. The igneous rocks of the Boganclough area, N.E. Scotland. *Scottish Journal of Geology* **9**, 165–76.

Comsti, M. E., Villones, R. I., Jr, De Jesus, C. V., Natividad, A. R., Rollen, L. A. & Dunroy, A. C. 1990. Mineralization at the Kelly gold mine, Baguio district, Philippines: fluid-inclusion and wall-rock alteration studies. *Journal of Geochemical Exploration* **35**, 341–62.

Coward, M. P. 1995. Structural and tectonic setting of Permo-Triassic basins of northwest Europe. *In* Boldy, S. A. R. (ed.) *Permian and Triassic Rifting in Northwest Europe. Geological Society, London, Special Publication* **91**, 7–39.

Curtis, S. F., Pattrick, R. A. D., Jenkin, G. R. T., Fallick, A. E., Boyce, A. J. & Treagus, J. E. 1993. Fluid inclusion and stable isotope study of fault-related mineralization in the Tyndrum area, Scotland. *Transactions of the Institution of Mining and Metallurgy (Section B Applied Earth Sciences)* **102**, B39–47.

De Ronde, C. E. J. & Blattner, P. 1988. Hydrothermal alteration, stable isotopes and fluid inclusions of the Goldern Cross epithermal gold deposit, Waihi, New Zealand. *Economic Geology* **83**, 895–917.

Diamond, L. W. 1994. Salinity of multivolatile fluid inclusions determined from clathrate hydrate stability. *Geochimica et Cosmochimica Acta* **58**, 19–41.

Drummond, S. E., Jr & Ohmoto, H. 1985. Chemical evolution and mineral deposition in boiling hydrothermal systems. *Economic Geology* **80**, 126–47.

Etoh, J., Izawa, E., Watanabe, K., Taguchi, S. & Sekine, R. 2002. Bladed quartz and its relationship to gold mineralization in the Hishikari low-sulfidation epithermal gold deposit, Japan. *Economic Geology* **97**, 1841–51.

Fournier, R. O. 1985. The behaviour of silica in hydrothermal solutions. *In* Berger, B. R. & Bethke, P. M. (eds.) *Geology and Geochemistry of Epithermal Systems. Reviews in Economic Geology* **2**, 45–60. El Paso, Texas: Society of Economic Geologists.

Fournier, R. O. 1991. The transition from hydrostatic to greater than hydrostatic fluid pressure in presently active continental hydrothermal systems in crystalline rock. *Geophysical Research Letters* **18**, 955–8.

Gallagher, M. J. 1991. *Regional Geochemistry of the East Grampians area*. Nottingham: British Geological Survey.

Giggenbach, W. F. 1997. The origin and evolution of fluids in magmatic-hydrothermal systems. *In* Barnes, H. L. (ed.) *The Geochemistry of Hydrothermal Ore Deposits*, 3rd edn, 737–96. Chichester: John Wiley and Sons.

Goldstein, R. H. 2001. Fluid inclusions in sedimentary and diagenetic systems. *Lithos* **55**, 159–93.

Gould, D. 1997. Geology of the country around Inverurie and Alford (Sheets 76E and 76W). *Memoir British Geological Survey*.

https://doi.org/10.1017/S0263593300000717 Published online by Cambridge University Press

Haas, J. L., Jr 1971. The effect of salinity and the maximum thermal gradient of a hydrothermal system at hydrostatic pressure. *Economic Geology* **57**, 940–6.
Heald, P., Foley, N. & Hayba, D. 1987. Comparative anatomy of volcanic-hosted epithermal deposits: acid-sulfate and adularia-sericite types. *Economic Geology* **82**, 1–26.
Hedenquist, J. W. & Henley, R. W. 1985. The importance of CO_2 on freezing point measurements of fluid inclusions: Evidence from active geothermal systems and implications for epithermal ore deposits. *Economic Geology* **80**, 1379–1406.
Henley, R. W. 1985. The geothermal framework for epithermal deposits. *In* Berger, B. R. & Bethke, P. M. (eds.) *Geology and Geochemistry of Epithermal Systems*. *Reviews in Economic Geology* **2**, 1–24.
Henley, R. W. & Ellis, A. J. 1983. Geothermal systems, ancient and modern. *Earth Science Reviews* **19**, 1–50.
Hillier, S. 1993. Origin, diagenesis, and mineralogy of chlorite minerals in Devonian lacustrine mudrocks, Orcadian Basin, Scotland. *Clays and Clay Minerals* **41**, 240–59.
Hiller, S. 2003. Quantitative analysis of clay and other minerals in sandstones by X-ray powder diffraction (XRPD). *International Association of Sedimentologists, Special Publication* **34**, 213–51.
Hillier, S. & Clayton, T. 1989. Illite/smectite diagenesis in Devonian lacustrine mudrocks from northern Scotland and its relationship to organic maturity indicators. *Clay Minerals* **24**, 181–96.
Inoue, A. 1995. Formation of clay minerals in hydrothermal environments. *In* Velde, B. (ed.) *Origin and Mineralogy of Clays*, 268–329. Berlin: Springer-Verlag.
Izawa, E., Urashima, Y., Ibaraki, K., Suzuki, R., Yokoyama, T., Kawasaki, K., Koga, A. & Taguchi, S. 1990. The Hishikari gold deposits: high-grade epithermal veins in Quaternary volcanics of southern Kyushu, Japan. *Journal of Geochemical Exploration* **36**, 1–56.
Jennings, S. & Thompson, G. R. 1986. Diagenesis of Plio-Pleistocene sediments of the Colorado River Delta, southern California. *Journal of Sedimentary Petrology* **56**, 89–98.
Kidston, R. & Lang, W. H. 1917. On Old Red Sandstone plants showing structure from the Rhynie Chert Bed, Aberdeenshire. Part I. *Rhynia Gwynne-Vaughani* Kidston & Lang. *Transactions of the Royal Society of Edinburgh* **51**, 761–84.
Krupp, R. E. & Seward, T. M. 1987. The Rotokawa geothermal system, New Zealand: an active epithermal gold-depositing environment. *Economic Geology* **82**, 1109–29.
Mackie, W. 1913. The rock series of Craigbeg and Ord Hill, Rhynie, Aberdeenshire. *Transactions of the Royal Society of Edinburgh* **10**, 205–36.
Norman, D. I., Harrison, R. W. & Andres, C. B. 1991. Geology and geochemical analysis of mineralizing fluids at the St. Cloud and US Treasury mines, Chloride mining district, New Mexico. *Journal of Geochemical Exploration* **42**, 61–89.
Oakes, C. S., Bodnar, R. J. & Simonson, J. M. 1990. The system $NaCl\text{-}CaCl_2\text{-}H_2O$: I. The ice liquidus at 1 atm. total pressure. *Geochimica et Cosmochimica Acta* **54**, 603–10.
Parnell, J. 1985. Evidence for evaporites in the Old Red Sandstone of Northern Scotland: replaced gypsum horizons in Easter Ross. *Scottish Journal of Geology* **21**, 377–80.
Rice, C. M., Ashcroft, W. A., Batten, D. J., Boyce, A. J., Caulfield, J. B. D., Fallick, A. E., Hole, M. J., Jones, E., Pearson, M. J., Rodgers, G., Saxton, J. M., Stuart, F. M., Trewin, N. H. & Turner, G. 1995. A Devonian auriferous hot spring system, Rhynie, Scotland. *Journal of the Geological Society, London* **152**, 229–50.
Rice, C. M., Trewin, N. H. & Anderson, L. I. 2002. Geological setting of the Early Devonian Rhynie cherts, Aberdeenshire, Scotland: an early terrestrial hot spring system. *Journal of the Geological Society, London* **159**, 203–14.
Rice, C. M. & Ashcroft, W. A. 2004. The geology of the northern part of the Rhynie Basin, Aberdeenshire, Scotland. *Transactions of the Royal Society of Edinburgh: Earth Sciences* **94** (for 2003), 299–308.
Rice, C. M. & Trewin, N. H. 1988. A Lower Devonian gold-bearing hot-spring system, Rhynie, Scotland. *Transactions of the Institution of Mining and Metallurgy (Section B Applied Earth Sciences)* **97**, B141–4.
Roedder, E. 1984. *Fluid inclusions*. *Reviews in Mineralogy* **12**. Mineralogical Society of America. 644 pp.
Scott, A. M. & Watanabe, Y. 1998. 'Extreme boiling' model for variable salinity of the Hokko low-sulfidation epithermal Au prospect, southwest Hokkaido, Japan. *Mineralium Deposita* **33**, 568–78.
Seward, T. M. & Barnes, H. L. 1997. Metal transport by hydrothermal ore fluids. *In* Barnes, H. L. (ed.) *The Geochemistry of Hydrothermal Ore Deposits*, 3rd end, 435–86. Chichester: John Wiley and Sons, 435–86.
Shepherd, T. J., Rankin, A. H. & Alderton, D. H. M. 1985. *A Practical Guide to Fluid Inclusion Studies*. London: Blackie.
Shikazono, N. & Nagayama, T. 1993. Origin and depositional mechanism of the Hishikari gold-quartz-adularia mineralization. *Resource Geology Special Issue* **14**, 47–56.
Simeone, R. & Simmons, S. F. 1999. Mineralogical and fluid inclusion studies of low-sulfidation epithermal veins at Osilo (Sardinia), Italy. *Mineralium Deposita* **34**, 705–17.
Simmons, S. F., Gemmell, J. B. & Sawkins, F. J. 1988. The Santo Nino silver lead zinc vein, Fresnillo District, Zacatecas, Mexico: Part II. Physical and chemical nature of ore forming solutions. *Economic Geology* **83**, 1619–41.
Simmons, S. F. & Browne, P. R. L. 1990. Mineralogic, alteration and fluid inclusion studies of epithermal gold-bearing veins at the Mt. Muro Prospect, Central Kalimantan (Borneo), Indonesia. *Journal of Geochemical Exploration* **35**, 63–103.
Simmons, S. F. & Browne, P. R. L. 1997. Saline fluid inclusions in sphalerite from the Broadlands-Ohaaki geothermal system: a coincidental trapping of fluids being boiled toward dryness. *Economic Geology* **92**, 485–9.
Simmons, S. F. & Browne, P. R. L. 2000. Hydrothermal minerals and precious metals in the Broadlands-Ohaaki geothermal system: implications for understanding low-sulfidation epithermal environments. *Economic Geology* **95**, 971–99.
Simon, G., Kesler, S. E., Ressell, N., Hall, C. M., Bell, D. & Pinero, E. 1999. Epithermal gold mineralization in an old volcanic arc: the Jacinto deposit, Camaguey district, Cuba. *Economic Geology* **94**, 487–506.
Simpson, M. P., Mauk, J. L. & Simmons, S. F. 2001. Hydrothermal alteration and hydrologic evolution of the Goldern Cross epithermal Au-Ag deposit, New Zealand. *Economic Geology* **96**, 773–96.
Trewin, N. H. 1994. Depositional environment and preservation of biota in the Lower Devonian hot-springs of Rhynie, Aberdeenshire. *Transactions of the Royal Society of Edinburgh: Earth Sciences* **84** (for 1993), 433–42.
Trewin, N. H. & Rice, C. M. 1992. Stratigraphy and sedimentology of the Devonian Rhynie chert locality. *Scottish Journal of Geology* **28**, 37–47.
Trewin, N. H. & Wilson, E. 2004. Correlation of the Early Devonian Rhynie chert beds between three boreholes at Rhynie, Aberdeenshire. *Scottish Journal of Geology* **40**, 73–81.
Ulrich, T., Gunther, D. & Heinrich, C. A. 1999. Gold concentration of magmatic brines and the metal budget of porphyry copper deposits. *Nature* **399**, 676–9.
Vityk, M. O. & Bodnar, R. J. 1995. Do fluid inclusions in high grade metamorphic terranes preserve peak metamorphic density during retrograde decompression? *American Mineralogist* **80**, 641–4.
Walderhaug, O. 1994. Temperatures of quartz cementation in Jurassic sandstones from the Norwegian continental shelf: evidence from fluid inclusions. *Journal of Sedimentary Research* **A64**, 311–23.
White, N. C., Leake, M. J., McCaughey, S. N. & Parris, B. W. 1995. Epithermal deposits of the southwest Pacific. *Journal of Geochemical Exploration* **54**, 87–136.
Wilkinson, J. J., Boyce, A. J., Earls, G. & Fallick, A. E. 1999. Gold remobilization by low-temperature brines: evidence from the Curraghinalt gold deposits, Northern Ireland. *Economic Geology* **94**, 289–96.

M. BARON, C. M. RICE, K. CZAPNIK and J. PARNELL, Department of Geology & Petroleum Geology, University of Aberdeen, Aberdeen, AB24 3UE, UK.
e-mail: m.baron@abdn.ac.uk

S. HILLIER, Macaulay Land Use Research Institute, Craigiebuckler, Aberdeen AB15 8QH, UK.

MS received 14 November 2003. Accepted for publication 16 August 2004.